Graphene nanoribbons epitaxy on boron nitride

Xiaobo Lu, Wei Yang, Shuopei Wang, Shuang Wu, Peng Chen, Jing Zhang, Jing Zhao, Jianling Meng, Guibai Xie, Duoming Wang, Guole Wang, Ting Ting Zhang, Kenji Watanabe, Takashi Taniguchi, Rong Yang, Dongxia Shi, and Guangyu Zhang

Citation: Applied Physics Letters **108**, 113103 (2016); doi: 10.1063/1.4943940
View online: http://dx.doi.org/10.1063/1.4943940
View Table of Contents: http://scitation.aip.org/content/aip/journal/apl/108/11?ver=pdfcov
Published by the AIP Publishing

Graphene nanoribbons epitaxy on boron nitride

Xiaobo Lu,[1] Wei Yang,[1,2] Shuopei Wang,[1] Shuang Wu,[1] Peng Chen,[1] Jing Zhang,[1] Jing Zhao,[1] Jianling Meng,[1] Guibai Xie,[1] Duoming Wang,[1] Guole Wang,[1] Ting Ting Zhang,[1] Kenji Watanabe,[3] Takashi Taniguchi,[3] Rong Yang,[1] Dongxia Shi,[1] and Guangyu Zhang[1,4,a)]
[1]*Beijing National Laboratory for Condensed Matter Physics and Institute of Physics, Chinese Academy of Sciences, Beijing 100190, China*
[2]*Laboratoire Pierre Aigrain, ENS-CNRS UMR 8551, Universités Pierre et Marie Curie and Paris-Diderot, 24 rue Lhomond, 75231 Paris Cedex 05, France*
[3]*National Institute for Materials Science, 1-1 Namiki, Tsukuba 305-0044, Japan*
[4]*Collaborative Innovation Center of Quantum Matter, Beijing 100190, China*

(Received 30 November 2015; accepted 18 February 2016; published online 14 March 2016)

In this letter, we report a pilot study on epitaxy of monolayer graphene nanoribbons (GNRs) on hexagonal boron nitride (h-BN). We found that GNRs grow preferentially from the atomic steps of h-BN, forming in-plane heterostructures. GNRs with well-defined widths ranging from ~15 nm to ~150 nm can be obtained reliably. As-grown GNRs on h-BN have high quality with a carrier mobility of ~20 000 cm^2 V^{-1} s^{-1} for ~100-nm-wide GNRs at a temperature of 1.7 K. Besides, a moiré pattern induced quasi-one-dimensional superlattice with a periodicity of ~15 nm for GNR/h-BN was also observed, indicating zero crystallographic twisting angle between GNRs and h-BN substrate. The superlattice induced band structure modification is confirmed by our transport results. These epitaxial GNRs/h-BN with clean surfaces/interfaces and tailored widths provide an ideal platform for high-performance GNR devices. © *2016 AIP Publishing LLC*.
[http://dx.doi.org/10.1063/1.4943940]

Graphene nanoribbons (GNRs) have recently attracted much interest for both fundamental research and practical applications due to their exotic electronic and spintronic properties.[1–6] It has been demonstrated that a confinement-induced gap can be opened in GNRs, and the gap depends strongly on the width and chirality of a GNR. Exceptional ballistic transport and room-temperature magnetic order were also observed in GNRs.[7,8] However, the fabrication of high quality intrinsic GNRs, which is critical for high performance GNR devices, remains a challenge. So far, GNRs have been successfully fabricated via various approaches including lithographic patterning of graphene,[6,9–13] carbon nanotubes unzipping,[14] exfoliation of graphite,[15] templated growth on SiC or metal surfaces,[16–18] and molecular self-assembly on metal surfaces.[19] However, fabrication of high-quality GNRs on certain substrates that can preserve GNRs' high quality as much as possible is still challenging. Typically, GNRs on SiO_2 substrates have very low carrier mobility, e.g., less than 2000 cm^2 V^{-1} s^{-1} at a width of ~100 nm, which limits their electronic applications. In general, to improve the quality of GNRs, several issues must be concerned. First, the substrate selection is quite important, since the electrical properties of GNRs on a dielectric layer are highly affected by the scattering from charge impurities,[20,21] and substrate surface roughness and phonons.[22–24] Second, clean surface and interface free of contaminations are necessary, since the impurities at surface and interface could cause severe scattering and doping of the 2D electron gas. Third, good lattice quality with low defect densities and proper edge passivations is undoubtedly essential. In this sense, we exploited epitaxy of GNRs on hexagonal boron nitride (h-BN). H-BN provides an excellent substrate for GNRs to preserve its high quality, owing to its atomically smooth surface, effectively reduced charge impurities and phonon scattering.[25] *In-situ* epitaxial growth guarantees a clean surface and interface with an edge passivation of hydrogen, as will be discussed below.

The epitaxial growth of GNRs on h-BN substrates was carried out via remote plasma enhanced chemical vapor deposition (r-PECVD). During growth, the methane molecules were dissociated by RF-plasma into active radicals to facilitate the growth of graphene.[26–28] Note that at a growth temperature of ~505 °C, single domain graphene can be grown on h-BN basal plane (refer to our previous results in Ref. 28). Interestingly, at lower growth temperatures, e.g., ~500 °C, the nucleation of graphene on the h-BN basal plane can be effectively suppressed due to the enhanced etching effect.[29,30] Therefore, graphene grows preferentially from the h-BN step edges, which serve as one dimensional seeds (Fig. 1(a)).

As-grown GNRs were characterized by Raman spectroscopy. Fig. 1(b) shows a Raman spectrum of a typical ~50-nm-wide GNR. The 2D peak, located at ~2668 cm^{-1}, could be fitted well with only one Lorentz peak, indicating the single-layer property of the GNR.[31,32] The characteristic peak of h-BN (at 1367 cm^{-1}) is quite close to the D peak of GNR (at 1336 cm^{-1}). The intensity ratio of D peak and G peak is ~0.6, indicating a high quality. Fig. 1(c) shows the atomic force microscope (AFM) images of an as-grown GNR with ultraclean surface. The topographic height of the as-grown GNR is ~0.4 nm, indicating a monolayer thickness. Fig. 1(d) shows the height distribution taken along the dashed green line in Fig. 1(c). Note that the height of GNRs on h-BN is larger than that of the monolayer h-BN interlayer spacing by ~0.1 nm. As-grown GNRs on h-BN show a trigonal moiré

a)Author to whom correspondence should be addressed. Electronic mail: gyzhang@aphy.iphy.ac.cn

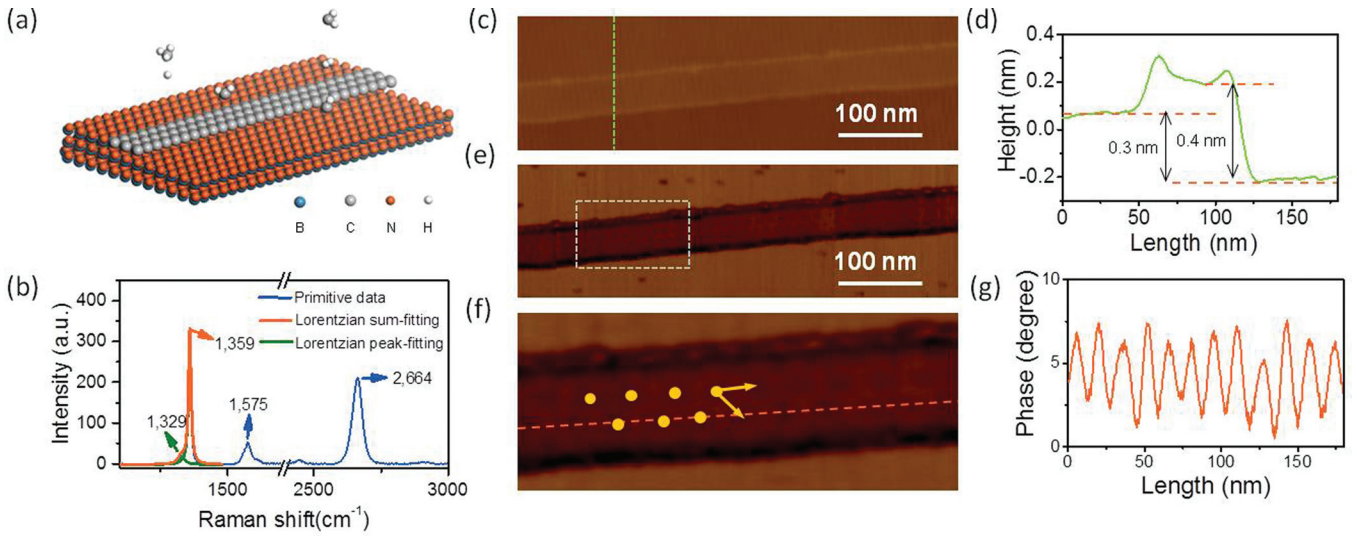

FIG. 1. Graphene nanoribbons epitaxy. (a) Schematic illustration of growth mechanism. (b) Raman spectrum of a typical 50-nm-wide as-grown GNR. (c) Height image of graphene nanoribbon measured by tapping mode AFM. (d) Cross-section of the height distribution taken along the dashed green line in (c). (e) Phase image of graphene nanoribbon related to (c). (f) Zoom-in phase image of the area in the dashed square in (e), showing triangular moiré pattern indicated by yellow dots. (g) Cross-section of the phase distribution taken alone the dashed orange line in (f) and averaged by ten lines.

pattern (Figs. 1(e) and 1(f)) originating from the lattice mismatch between graphene and the supporting h-BN substrate. Fig. 1(g) shows the phase distribution taken alone the dashed orange line in Fig. 1(f) and averaged by ten lines. The periodicity of the moiré pattern is about 15 nm, corresponding to the zero crystallographic rotation angle between GNRs and the supporting h-BN substrate.[28,33] As shown in Fig. 1(e), the long-range periodicity of the moiré pattern was destroyed in the transverse direction while preserved well in longitudinal direction, forming a quasi-one-dimensional moiré superlattice. The chirality of as-grown GNRs could thus be obtained from the observed moiré pattern's orientation, which is always the same with the lattice orientation of graphene or h-BN. Atomic-resolution AFM was also used to characterize the as-grown GNRs. Fig. 2(a) shows a typical GNR with a width of ~15 nm. Fig. 2(b) shows the zoomed-in image of Fig. 2(a) at the interface area. According to Fig. 2(a), graphene shares the same lattice orientation with h-BN, which is another solid evidence of the epitaxial growth. Note that the interface configuration between two gray lines is not shown clearly. It is difficult to achieve atomic resolution imaging at the interface area mainly because the height of GNRs on h-BN is larger than that of the monolayer h-BN interlayer spacing by ~0.1 nm. Fig. 2(c) is a zoomed-in image showing a typical honeycomb lattice of graphene. Grain boundaries or line defects were barely seen.

During the growth of GNRs, hexagonal graphene domains were also formed on the h-BN surface. The orientation of as-grown GNRs could also be determined by the orientation of these hexagonal domains, which have zigzag edges.

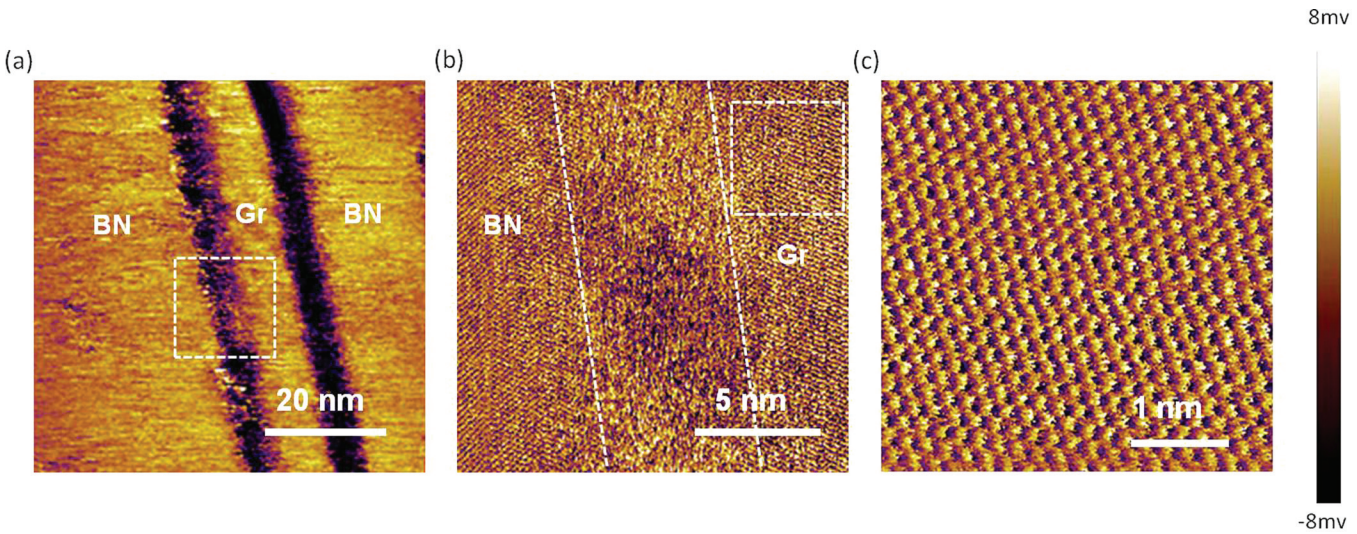

FIG. 2. Investigation on graphene/h-BN lateral interface. (a) Lateral image of a ~15 nm GNR measured by contact mode AFM. The scale bar is 20 nm. (b) Zoom-in lateral image of the lateral area in the dashed square in (a). The interface area is between the two dashed gray lines. The scale bar is 5 nm. (c) Zoom-in image of the area in the dashed square in (b).

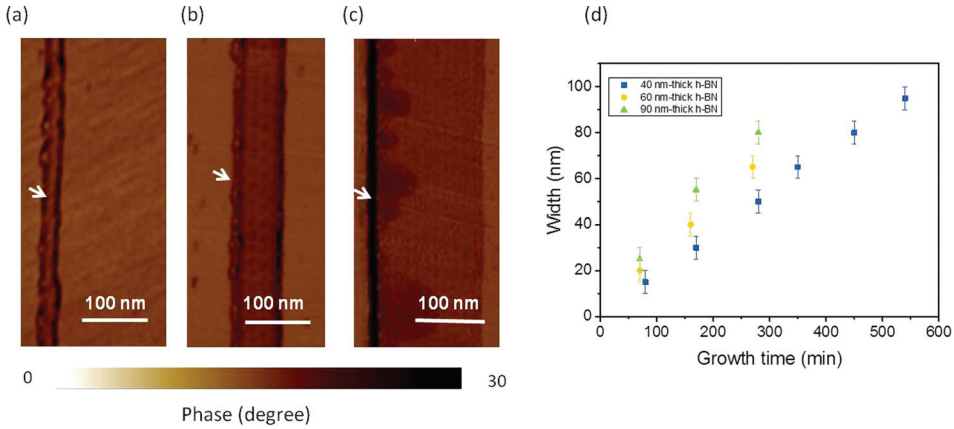

FIG. 3. GNRs with different widths tuned by growth time. (a)–(c) Phase images of as-grown graphene nanoribbons with different widths. The white arrows in (a)–(c) indicate the one-dimensional graphene/h-BN interface. All the phase images are measured by tapping mode AFM with graphene shown in dark colour. The scale bars in (a)–(c) are 100 nm. (d) The growth duration dependence of the thickness of h-BN flakes.

GNRs grown along the zigzag orientation are the best in terms of smooth edges.[34] By employing different growth durations, we thus grew a series of zigzag-oriented GNRs with widths ranging from 15 nm to 150 nm and a few typical samples are shown in Figs. 3(a)–3(c). In Fig. 3(d), we plotted the widths of GNRs on 40, 60, and 90 nm-thick h-BN as a function of growth time. We can see that the widths of GNRs increase linearly with the growth time. It was also found that graphene could hardly be grown on the h-BN flakes with the thickness of <30 nm. In principle, the fluctuation of the h-BN substrate was energetically unfavorable for epitaxial growth of graphene. A thin h-BN flake (thickness below 30 nm) could not effectively screen the fluctuation of the SiO_2 surface[34] The growth rate, about 0.2 nm/min on 40-nm-thick h-BN flakes, increased to 0.3 nm/min on 90-nm-thick h-BN flakes. However, the growth rate shows no obvious change when the thickness of h-BN flakes is above 90 nm, suggesting a full screening of the SiO_2 surface fluctuations.

To characterize the electrical properties of as-grown GNRs, we fabricated three terminal devices based on as-grown GNRs with 10 nm-Pd/50 nm-Au as contact metal, heavily *p*-doped silicon as back gate, and 100 nm silicon oxide layer as gate dielectrics. Electrical transport measurements were carried out in a cryogenic Dewar via a standard lock-in technique. For a ~100-nm-wide GNR in zigzag orientation (channel length of ~500 nm), the resistance (R) versus gate voltage (Vg) at different temperature was shown in Fig. 4(a). The Dirac point (DP) is at $Vg \approx -2$ V, suggesting a slight hole doping from the h-BN substrate. The estimated carrier mobility near charge neutral point was ~20 000 $cm^2\ V^{-1}\ s^{-1}$ at 1.7 K, indicating very high quality of the as-grown GNR. The estimated room temperature field-effect mobility in this work in comparison with other previously results is shown in Fig. 4(b).[6,17,18,35] The field-effect mobility of as-grown GNRs ranged from ~1000 to ~4000 $cm^2\ V^{-1}\ s^{-1}$ at room temperature depending on

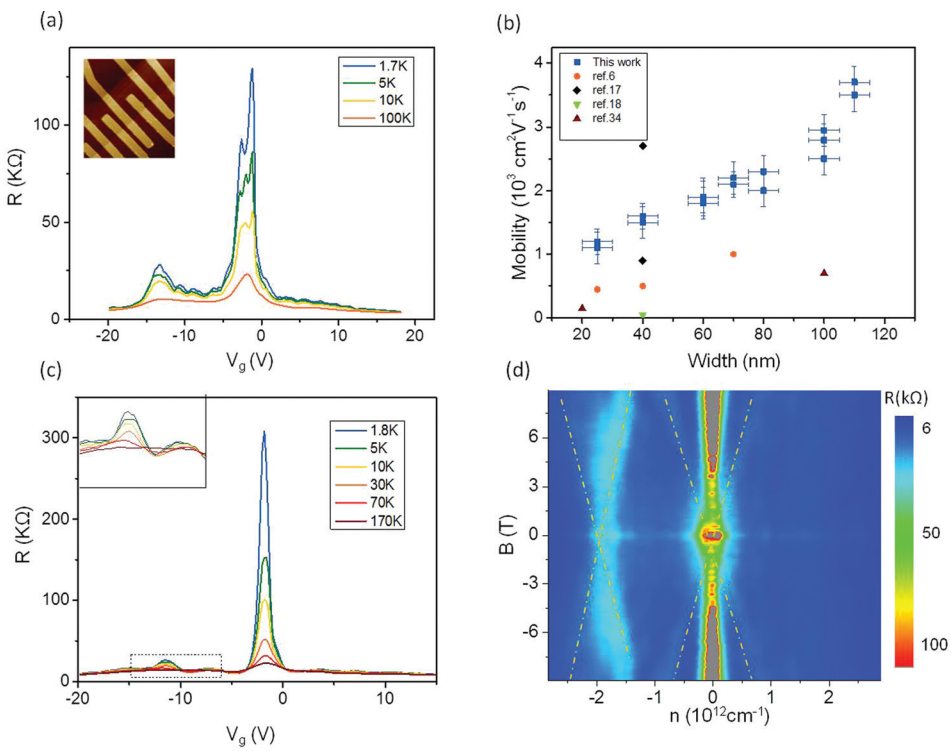

FIG. 4. Transport measurements of as-grown graphene nanoribbon. (a) Resistance of ~100-nm wide GNR versus applied gate voltage at different temperature. Inset is the AFM image of as-fabricated device. (b) Statistic mobility of as-grown GNRs and other previously reported works. (c) Resistance versus applied gate voltage at B = 9 T. (d) Two-terminal magnetoresistance versus applied gate voltage and magnetic field.

the widths of as-grown GNRs, comparable to the highest value reported.[17]

Besides the resistance peak at Dirac point, two satellite peaks were also observed due to the moiré superlattice modulations.[28,33,36–38] In consistent with previous results, the satellite peak in the hole branch was stronger than that in electron branch.[28,36–38] The asymmetry could be attributed to the pseudospin mixing potential in graphene moiré superlattice on h-BN.[39] Fig. 4(c) shows R-Vg curves at a perpendicular magnetic field of B = 9 T. As temperature decreases, the superlattice Dirac point (SDP) in the hole branch exhibited complicated features as shown in the inset. To closely see the features near the SDP, we plotted the magnetoresistance versus Vg and magnetic field B in Fig. 4(d). A standard fan diagram for quantum hall effect in graphene is shown, and the plateaus associated with both DP and SDP at filling factor of 2 can be distinguished. The SDP persisted even the width of GNRs down to 25 nm, indicating that the band structure of as-grown GNRs could be effectively modified by the quasi-one-dimensional moiré potential mentioned above.[34] More experiments are still underway to investigate the properties of as-grown quasi-one-dimensional superlattice system.

In conclusion, we have achieved epitaxy of monolayer GNRs on h-BN with tailored widths ranging from 15 nm to 150 nm. As-grown GNRs exhibited high quality with a carrier mobility of $\sim$20 000 $cm^2\ V^{-1}\ s^{-1}$ at a width of $\sim$100 nm. The transport results also revealed the band structure modulation induced by the quasi-one-dimensional moiré superlattice. Our method could solve the critical issues associated with absolutely clean surface/interface for GNRs, which may help to provide an ideal platform for GNR devices.

Epitaxial growth of GNRs. Single-crystal h-BN flakes were first exfoliated onto a 100 nm-SiO_2/P^{++}Si substrate by mechanical cleaving method. Before growth, the substrate was annealed in pure CH_4 atmosphere at a growth temperature of $\sim$500 °C (the growth temperature of single-domain graphene is about $\sim$505 °C) in r-PECVD system for at least 30 min to remove the tape residues. Then, the growth process was carried out in a flow of 30 sccm methane with a gas pressure 0.2 Torr, plasma power 110 W.

Atomic force microscopy characterizations. AFM images in Figs. 1 and 3 were taken by tapping mode AFM (Multimode IIId, Veeco Instruments) at room temperature under ambient conditions. The atomic-resolution images in Fig. 2 were taken by contact mode AFM (Cypher S) at room temperature under ambient condition. To reduce the influence of thermal drift, the scan rate was set to a high value ranging from 20 to 50 Hz.

Raman spectroscopy characterizations. Raman spectroscopy was performed in a Horiba Jobin Yvon LavRam HR-Evolution Raman microscope using a 532-nm HeNe laser (spot size $\sim$1 μm, power 10 mW). The integration time of the spectrum for a single GNR was set to be 60 s to increase the intensity of signal.

Device fabrication and transport measurements for as-grown GNRs. As-grown GNRs were located by AFM before the source-drain electrode pattern was defined through electron beam lithography process. Contact metal (10 nm-Pd/50 nm-Au) was deposited through electron beam evaporation. Before measurements, the devices were annealed in pure argon atmosphere at 250 °C for 1 h to improve the electrical contact quality. Electrical transport measurements were performed in a cryogenic Dewar via a standard lock-in technique.

This work was supported by the National Basic Research Program of China (973 Program) under Grant Nos. 2013CB934500 and 2012CB921302, the National Science Foundation of China (NSFC, Grant Nos. 91223204, 91323304, 61325021, 61390503, and 11574361), and Strategic Priority Research Program (B) of the Chinese Academy of Sciences (Grant No. XDB0710100).

The authors declare no competing financial interest.

[1]K. Nakada, M. Fujita, G. Dresselhaus, and M. S. Dresselhaus, Phys. Rev. B **54**, 17954 (1996).
[2]Y. W. Son, M. L. Cohen, and S. G. Louie, Phys. Rev. Lett. **97**, 216803 (2006).
[3]S. Y. Woo, M. L. Cohen, and S. G. Louie, Nature **444**, 347 (2006).
[4]B. Trauzettel, D. V. Bulaev, D. Loss, and G. Burkard, Nat. Phys. **3**, 192 (2007).
[5]V. Barone, O. Hod, and G. E. Scuseria, Nano Lett. **6**, 2748 (2006).
[6]M. Y. Han, B. Oezyilmaz, Y. Zhang, and P. Kim, Phys. Rev. Lett. **98**, 206805 (2007).
[7]J. Baringhaus, M. Ruan, F. Edler, A. Tejeda, M. Sicot, A. T. Ibrahimi, A. P. Li, Z. Jiang, E. H. Conrad, C. Berger, C. Tegenkamp, and W. A. de Heer, Nature **506**, 349 (2014).
[8]G. Z. Magda, X. Jin, I. Hagymasi, P. Vancso, Z. Osvath, P. N. Incze, C. Hwang, L. P. Biro, and L. Tapaszto, Nature **514**, 608 (2014).
[9]L. Tapaszto, G. Dobrik, P. Lambin, and L. P. Biro, Nat. Nanotechnol. **3**, 397 (2008).
[10]J. Bai, X. Duan, and Y. Huang, Nano Lett. **9**, 2083 (2009).
[11]R. Yang, L. Zhang, Y. Wang, Z. Shi, D. Shi, H. Gao, E. Wang, and G. Zhang, Adv. Mater. **22**, 4014 (2010).
[12]Z. Shi, R. Yang, L. Zhang, Y. Wang, D. Liu, D. Shi, E. Wang, and G. Zhang, Adv. Mater. **23**, 3061 (2011).
[13]G. Xie, Z. Shi, R. Yang, D. Liu, W. Yang, M. Cheng, D. Wang, D. Shi, and G. Zhang, Nano. Lett. **12**, 4642 (2012).
[14]L. Jiao, L. Zhang, X. Wang, G. Diankov, and H. Dai, Nature **458**, 877 (2009).
[15]X. Li, X. Wang, L. Zhang, S. Lee, and H. Dai, Science **319**, 1229 (2008).
[16]Z. Liu, L. L. Ma, G. Shi, Z. Wu, Y. J. Gong, S. D. Lei, X. B. Yang, J. G. Zhang, J. J. Yu, K. P. Hackenberg, A. Babakhani, J. C. Idrobo, R. Vajtai, L. Jun, and P. M. Ajayan, Nat. Nanotechnol. **8**, 119 (2013).
[17]M. Sprinkle, M. Ruan, Y. Hu, J. Hankinson, M. Rubio-Roy, B. Zhang, X. Wu, C. Berger, and W. A. de Heer, Nat. Nanotechnol. **5**, 727 (2010).
[18]T. Kato and R. Hatakeyama, Nat. Nanotechnol. **7**, 651 (2012).
[19]J. Cai, P. Ruffieux, R. Jaafar, M. Bieri, T. Braun, S. Blankenburg, M. Muoth, A. P. Seitsonen, M. Saleh, X. Feng, K. Muellen, and R. Fasel, Nature **466**, 470 (2010).
[20]E. H. Hwang, S. Adam, and S. D. Sarma, Phys. Rev. Lett. **98**, 186806 (2007).
[21]J. H. Chen, C. Jang, S. Xiao, M. Ishigami, and M. S. Fuhrer, Nat. Nanotechnol. **3**, 206 (2008).
[22]M. Ishigami, J. H. Chen, W. G. Cullen, M. S. Fuhrer, and E. D. Williams, Nano Lett. **7**, 1643 (2007).
[23]S. V. Morozov, K. S. Novoselov, M. I. Katsnelson, F. Schedin, D. C. Elias, J. A. Jaszczak, and A. K. Geim, Phys. Rev. Lett. **100**, 016602 (2008).
[24]S. Fratini and F. Guinea, Phys. Rev. B **77**, 195415 (2008).
[25]C. R. Dean, A. F. Young, I. Meric, C. Lee, L. Wang, S. Sorgenfrei, K. Watanabe, T. Taniguchi, P. Kim, K. L. Shepard, and J. Hone, Nat. Nanotechnol. **5**, 722 (2010).
[26]L. Zhang, Z. Shi, Y. Wang, R. Yang, D. Shi, and G. Zhang, Nano Res. **4**, 315 (2011).
[27]L. Zhang, Z. Shi, D. Liu, R. Yang, D. Shi, and G. Zhang, Nano Res. **5**, 258 (2012).
[28]W. Yang, G. Chen, Z. Shi, C. Liu, L. Zhang, G. Xie, M. Cheng, D. Wang, R. Yang, D. Shi, K. Watanabe, T. Taniguchi, Y. Yao, Y. Zhang, and G. Zhang, Nat. Mater. **12**, 792 (2013).
[29]L. Zhang, M. Ni, D. Liu, D. Shi, and G. Zhang, J. Phys. Chem. C **116**, 26929 (2012).
[30]D. Liu, W. Yang, L. Zhang, J. Zhang, J. Meng, R. Yang, G. Zhang, and D. Shi, Carbon **72**, 387 (2014).

[31]A. C. Ferrari, J. C. Meyer, V. Scardaci, C. Casiraghi, M. Lazzeri, F. Mauri, S. Piscanec, D. Jiang, K. S. Novoselov, S. Roth, and A. K. Geim, Phys. Rev. Lett. **97**, 187401 (2006).
[32]D. Graf, F. Molitor, K. Ensslin, C. Stampfer, A. Jungen, C. Hierold, and L. Wirtz, Nano Lett. **7**, 238 (2007).
[33]M. Yankowitz, J. Xue, D. Cormode, J. D. Sanchez-Yamagishi, K. Watanabe, T. Taniguchi, P. Jarillo-Herrero, P. Jacquod, and B. J. LeRoy, Nat. Phys. **8**, 382 (2012).
[34]See supplementary material at http://dx.doi.org/10.1063/1.4943940 for GNRs with different directions, surface topography of h-BN of different thickness, transport measurements of GNRs with different widths.
[35]M. El Gemayel, A. Narita, L. F. Doessel, R. S. Sundaram, A. Kiersnowski, W. Pisula, M. R. Hansen, A. C. Ferrari, E. Orgiu, X. Feng, K. Muellen, and P. Samor, Nanoscale **6**, 6301 (2014).
[36]L. A. Ponomarenko, R. V. Gorbachev, G. L. Yu, D. C. Elias, R. Jalil, A. A. Patel, A. Mishchenko, A. S. Mayorov, C. R. Woods, J. R. Wallbank, M. M. Kruczynski, B. A. Piot, M. Potemski, I. V. Grigorieva, K. S. Novoselov, F. Guinea, V. I. Fal'ko, and A. K. Geim, Nature **497**, 594 (2013).
[37]C. R. Dean, L. Wang, P. Maher, C. Forsythe, F. Ghahari, Y. Gao, J. Katoch, M. Ishigami, P. Moon, M. Koshino, T. Taniguchi, K. Watanabe, K. L. Shepard, J. Hone, and P. Kim, Nature **497**, 598 (2013).
[38]B. Hunt, J. D. S. Yamagishi, A. F. Young, M. Yankowitz, B. J. LeRoy, K. Watanabe, T. Taniguchi, P. Moon, M. Koshino, P. J. Herrero, and R. C. Ashoori, Science **340**, 1427 (2013).
[39]Z. Shi, C. Jin, W. Yang, L. Ju, J. Horng, X. Lu, H. A. Bechtel, M. C. Martin, D. Fu, J. Wu, K. Watanabe, T. Taniguchi, Y. Zhang, X. Bai, E. Wang, G. Zhang, and F. Wang, Nat. Phys. **10**, 743 (2014).